LIMNOLOGY and OCEANOGRAPHY

ASLO

Limnol. Oceanogr. 66, 2021, 2901–2913

doi: 10.1002/lno.11799

Submesoscale physicochemical dynamics directly shape bacterioplankton community structure in space and time

Eduard Fadeev,[1,2*,a] **Matthias Wietz**,[1,2] **Wilken-Jon von Appen**,[1] **Morten H. Iversen**,[1,3] **Eva-Maria Nöthig**,[1] **Anja Engel**,[4] **Julia Grosse**,[4] **Martin Graeve**,[1] **Antje Boetius**[1,2,3]

[1]Alfred Wegener Institute, Bremerhaven, Germany
[2]Max Planck Institute for Marine Microbiology, Bremen, Germany
[3]MARUM, University of Bremen, Bremen, Germany
[4]GEOMAR Helmholtz Centre for Ocean Research, Kiel, Germany

Abstract

Submesoscale eddies and fronts are important components of oceanic mixing and energy fluxes. These phenomena occur in the surface ocean for a period of several days, on scales between a few hundred meters and few tens of kilometers. Remote sensing and modeling suggest that eddies and fronts may influence marine ecosystem dynamics, but their limited temporal and spatial scales make them challenging for observation and in situ sampling. Here, the study of a submesoscale filament in summerly Arctic waters (depth 0–400 m) revealed enhanced mixing of Polar and Atlantic water masses, resulting in a ca. 4 km wide and ca. 50 km long filament with distinct physical and biogeochemical characteristics. Compared to the surrounding waters, the filament was characterized by a distinct phytoplankton bloom, associated with depleted inorganic nutrients, elevated chlorophyll *a* concentrations, as well as twofold higher phyto- and bacterioplankton cell abundances. High-throughput 16S rRNA gene sequencing of bacterioplankton communities revealed enrichment of typical phytoplankton bloom-associated taxonomic groups (e.g., *Flavobacteriales*) inside the filament. Furthermore, linked to the strong water subduction, the vertical export of organic matter to 400 m depth inside the filament was twofold higher compared to the surrounding waters. Altogether, our results show that physical submesoscale mixing can shape distinct biogeochemical conditions and microbial communities within a few kilometers of the ocean. Hence, the role of submesoscale features in polar waters for surface ocean biodiversity and biogeochemical processes need further investigation, especially with regard to the fate of sea ice in the warming Arctic Ocean.

Microbial communities perform key functions in marine biogeochemical cycles and energy fluxes (Azam and Malfatti 2007; Buchan et al. 2014). Linking these microbial activities with their distributional patterns is required for a better understanding of organic matter transformations and associated ecological dynamics. To date, the regional biogeography of pelagic microbial communities is mostly attributed to larger-scale (> 50 km) processes of physical mixing (Fuhrman et al. 2006). However, there is increasing evidence that mesoscale eddies and frontal systems have important ecological functions, featuring elevated phytoplankton growth (Lévy et al. 2001; Mouriño 2004; Thomsen et al. 2016), unique bacterioplankton communities (Nelson et al. 2014; Baltar et al. 2016; Djurhuus et al. 2017) and high microbial activity (Baltar et al. 2007; Baltar et al. 2010; Baltar and Arístegui 2017). Thus, physical oceanic dynamics on small spatial scales presumably influence the composition and activity of bacterioplankton communities and therefore directly impact biogeochemical processes.

In recent years, observations by satellite remote sensing, autonomous profiling floats, and towed instruments revealed the ubiquity of submesoscale features in the global ocean,

*Correspondence: eduard.fadeev@univie.ac.at

Additional Supporting Information may be found in the online version of this article.

[a]Present address: Department of Functional and Evolutionary Ecology, University of Vienna, Vienna, Austria

Author Contribution Statement: EF analyzed the data and wrote the manuscript with guidance from AB, WJvA and MW. WJvA conducted the physical oceanography sampling. MHI conducted the free-drifting sediment traps measurements. EMN and MG conducted the biogeochemical measurements. EMN contributed microscopic counts of phyto- and protozooplankton. AE and JG contributed bacterioplankton cell counts. All authors contributed to the final version of the manuscript.

confirming previous hypotheses based on numerical models (Ferrari 2011; Lévy et al. 2012; Thompson et al. 2016). These oceanic motions in surface waters are due to horizontal density gradients, taking the shape of eddies and filaments with a lateral spatial range between a few hundred meters and some tens of kilometers (Sasaki et al. 2014). Their motions persist for up to several days, characterized by strong lateral currents along the filament and an increased vertical circulation (McWilliams 2016). The relatively small spatial scale and short-lived nature of such phenomena make them challenging for in situ biological observations (e.g., molecular sampling). To date, biological observations from oceanic submesoscale filaments have been focused on phyto- and zooplankton (reviewed in Lévy et al. 2018), whereas almost nothing is known about bacterioplankton communities in these filaments despite their ecological relevance (Baltar et al. 2009, 2016; Baltar and Arístegui 2017).

The Fram Strait is the main gateway between the North Atlantic and Arctic Oceans. The Strait harbors of two major surface current systems: (1) the East Greenland Current flowing southwards along the Greenland shelf, transporting cold Polar water and sea ice to the North Atlantic (de Steur et al. 2009); and (2) the West Spitsbergen Current flowing northwards along the Svalbard Archipelago, transporting relatively warm and saline Atlantic water into the Arctic Ocean (Beszczynska-Möller et al. 2012; von Appen et al. 2016). The interactions between these distinct water masses result in a baroclinic instability in the central Fram Strait which facilitates subduction of Atlantic water below the Polar water (von Appen et al. 2016; Wulff et al. 2016; Wekerle et al. 2017). Investigating oceanographic dynamics in the Fram Strait is of importance considering the relevance of interacting water masses for the "Atlantification" of the Arctic Ocean (Randelhoff et al. 2018; Wang et al. 2020). In addition to physicochemical differences, the Polar and the Atlantic water masses harbor distinct bacterioplankton communities (Wilson et al. 2017; Fadeev et al. 2018; Müller et al. 2018). Thus, this region provides an excellent opportunity to investigate how bacterioplankton communities are shaped by submesoscale processes between distinct water masses and how these patterns correspond to the general microbial distribution in the Fram Strait.

Here, we explored biological responses to the physicochemical processes within a submesoscale filament in the central Fram Strait, formed as a result of a strong salinity gradient between Atlantic and Polar waters close to the ice edge (von Appen et al. 2018). Using a set of measured parameters, embedded into a high-resolution physical analysis of the filament (von Appen et al. 2018) which we briefly summarize below, we investigated how the submesoscale processes impacted nutrient distribution, phyto- and bacterioplankton community composition, and downward export of particulate organic matter (POC) from the filament. We studied free-living (0.22–3 μm) and particle-associated (>3 μm) bacterial and archaeal communities (further addressed as bacterioplankton) inside and outside the filament, at six depths from surface (10 m) to mesopelagic (400 m) waters. This allowed comparisons of bacterioplankton communities inside and outside the filament, and evaluation of the extent the observed differences resulted from mixing between water masses or internal succession within the communities. Specifically, we tested the hypothesis that submesoscale variations in phytoplankton and bacterioplankton communities directly correspond with the observed environmental gradients within the filament and surrounding waters. Further insights into the biological dynamics associated with such ubiquitous submesoscale features are needed to upscale their impact on ecosystem productivity and functioning in polar seas.

Materials and methods

Water sampling and metadata collection

Sampling was carried out in July 2017 during RV Polarstern expedition PS107 using 12 L Niskin bottles mounted on a CTD rosette (SBE 911 plus probe; Sea-Bird Electronics, Bellevue, WA) equipped with double temperature and conductivity sensors, a pressure sensor, altimeter, chlorophyll *a* fluorometer and transmissometer. Hydrographic data, including temperature and salinity are available at PANGAEA (doi: 10.1594/PANGAEA.894189). At all stations, water samples were collected at five depths: 10, 20–30, 50, 100, 200, and 400 m (Supporting information Table S1).

Concentrations of inorganic nutrients

Inorganic nutrients were analyzed with a continuous flow autoanalyzer (Evolution III, Alliance Instruments, Salzburg, Austria) directly on board after sampling. Phosphate, silicate, nitrate, nitrite, and ammonium were measured in technical duplicates of unfiltered CTD samples simultaneously on five channels, following Grasshoff et al. (2009). Ammonium was quantified using fluorescence spectroscopy after Kérouel and Aminot (1997). All measurements were calibrated with a five nutrients standard cocktail (traceable to SRM from NIST; Merck, Darmstadt, Germany) diluted in artificial seawater (ASW), which was also used as wash-water between the samples. Each 20th run we checked our standards with Reference Material for Nutrients in Seawater (CRM 7602-a; National Meteorology Institute of Japan, Japan). Standards and methods have been proven by inter-calibration exercises (e.g., ICES and Quasimeme). Detection limits: nitrate [NO_3^-] 0.02 μmol L^{-1}; nitrite [NO_2^-] 0.002 μmol L^{-1}; phosphate [PO_4^{3-}] 0.01 μmol L^{-1}; silicate [$Si(OH)_4$] 0.03 μmol L^{-1}; ammonium [NH_4^+] 0.01–0.02 μmol L^{-1}.

The underway measurements of pCO_2 were retrieved from the SOCAT database (www.socat.info), under expedition code 06AQ20170723.

Concentrations of chlorophyll *a*, particulate organic carbon and biogenic silica

Concentrations of chlorophyll *a* (chl-*a*) were determined from 0.5 to 2 L of seawater filtered onto glass fiber filters (GF/F; Whatman plc, Maidstone, UK) under low vacuum pressure (<200 mbar). Filters were stored at −20°C until analysis. Pigments were extracted, using plastic vials, with 10 mL of 90% acetone. The filters treated with an ultrasonic device in an ice bath for <1 min, and then further extracted in the refrigerator for 2 h. Subsequently filters were centrifuged for 10 min at 5000 rpm at 4°C prior to measurement. The concentration was determined using glass vials fluorometrically (Turner Designs, CA), together with total phaeophytin concentration after acidification (HCl, 0.1 N) based on Edler (1979) and Evans and O'Reilly (1982), respectively. The standard deviation of replicate test samples was <10%.

Particulate organic carbon (POC) was determined from 0.75 to 2 L of seawater filtered onto pre-combusted (4 h at 500°C) glass fiber filters (GF/F; Whatman plc, Maidstone, UK) at low vacuum (<200 mbar). After filtration, the filters were stored frozen at −20°C until analysis. Prior to analysis, filters were soaked in 0.1 N HCl for removal of inorganic carbon and dried at 60°C. POC concentrations were determined with a CHN Elemental Analyzer by Carlo Erba (ThermoFisher Scientific, Rockford, IL).

Particulate biogenic silica (PbSi) was determined following von Bodungen et al. (1991). Subsamples of 0.5–1 L were filtered on cellulose acetate filters (0.8 μm pore size), processed using the wet-alkaline method (with 0.2 M NaOH pretreated 12 h at 85°C in an oven), and extracted for 2 h at 85°C in a shaking water bath.

Microscopic counts of phytoplankton groups

Seawater samples from 10 and 20–30 m depths were preserved in hexamethylenetetramine-buffered formalin (final concentration 0.5%) and stored in brown glass bottles. Phytoplankton cells were counted by light microscopy. For microscopic analyses an aliquot of 50 mL was transferred to settling chambers where cells were allowed to settle for 48 h. Phytoplankton cells were identified to genus level and at least 500 cells (50–100 per major group; up to 1000 for *Phaeocystis*) were counted with an inverted microscope at three different magnifications using phase contrast.

Phytoplankton carbon content (PPC) was calculated by multiplying cell counts with the carbon value for individual cells following Edler (1979).

Bacterioplankton cell abundances

Cell abundances were determined by FACSCalibur flow cytometry (Becton Dickinson, Franklin Lakes, NJ). Samples were fixed with glutaraldehyde at 1% final concentration and stored at −20°C. The samples were stained with SYBRGreen I (Invitrogen, Carlsbad, CA) prior to analysis and enumerated in side scatter vs. green fluorescence cytograms. Polyscience fluorescent latex beads (Becton Dickinson, Franklin Lakes, NJ) were used to normalize the counted events to volume (Gasol and Del Giorgio 2000).

Export of particulate organic carbon

Export flux of particulate organic carbon (POC) was determined via free-drifting sediment traps at 100, 200, and 400 m at the centre (station T1) and the south-eastern edge of the filament (station T3). The samples were split into eight subsamples using a McLane Wet Sample Divider (McLane Research Laboratories, Falmouth, MA) with deviation between aliquots <5.0%. One subsample per depth and sediment trap deployment for POC analyses. Zooplankton swimmers were removed manually under a microscope before filtration on pre-combusted GF/F filters (Whatman plc, Maidstone, UK). Filters were fumed with concentrated hydrochloride acid (HCl, 37%) for 24 h and dried for 48 h at 40°C before packing into tin cartridges and analysis on a EuroEA Elemental Analyzer (precision of ±0.7 μg C or ±0.3%; HEKAtech, Wegberg, Germany). Blank filters were used to correct for contaminations.

DNA isolation and 16S rRNA gene amplicon sequencing

For assessing archaeal and bacterial community composition 2–4 L of seawater were filtered with a peristaltic pump (Masterflex; Cole Parmer, Vernon Hills, IL) through successive membrane filters of 3 μm (Nucleopore 47 mm polycarbonate; Whatman plc, Maidstone, UK) and 0.22 μm (Sterivex; Merck, Darmstadt, Germany) pore sizes to obtain particle-associated (PA) and free-living (FL) communities, respectively. All samples were stored at −20°C until DNA isolation. Genomic DNA was isolated by a combined chemical and mechanical procedure using the PowerWater DNA Isolation Kit (QIAGEN, Hilden, Germany). Sterivex cartridges were cracked open and filters transferred to kit-supplied bead beating tubes. The isolation was continued according to the manufacturer's instructions, and DNA was stored at − 20°C. Library preparation was performed according to the standard instructions of the 16S Metagenomic Sequencing Library Preparation protocol (Illumina, San Diego, CA). The hypervariable V4-V5 region of 16S rRNA genes was amplified using primers 515F-Y (5′-GTGYCAGCMGCCGCGGTAA-3′) and 926R (5′-CCGYCAATTY MTTTRAGTTT-3′; Parada et al. 2016). Sequences were obtained on the Illumina HiSeq platform in a 2 × 250 bp paired-end run (CeBiTec, Bielefeld, Germany) following the standard instructions of the 16S Metagenomic Sequencing Library Preparation protocol (Illumina, San Diego, CA).

Bioinformatics and statistical analyses

Raw paired-end reads were primer-trimmed using cutadapt (Martin 2011). Further analyses were conducted using R v3.6.3 (http://www.R-project.org/) in RStudio v1.2.5033 (www.rstudio.org). Trimmed reads were classified into amplicon sequence variants (ASVs) using DADA2 v1.14.1 (Callahan et al. 2016) following the tutorial (https://benjjneb.github.io/dada2/tutorial.html). Briefly, chimeras and singletons were

filtered and produced amplicon sequence variants (ASVs) taxonomically classified using Silva reference database release 138 (Quast et al. 2013). The ASVs taxonomically unclassified at phylum level, as well as the ASVs assigned to mitochondria and chloroplast, were excluded from further analysis.

Sample data matrices were managed using R package "phyloseq" v1.28.0 (McMurdie and Holmes 2013) and plots were generated using R package "ggplot2" v3.3.0 (Gómez-Rubio 2017). Rarefaction analysis was conducted using R package "iNEXT" v2.0.20 (Hsieh et al. 2016). Calculation and visualization of shared and unique ASVs was conducted using R package "venn" v1.9 (Dusa 2020). Statistical tests were conducted using R package "vegan" v2.5.6 (Oksanen et al. 2019). Prior to downstream analysis, a prevalence threshold (i.e., in how many samples did an ASV appear at least once) of 5% was applied on the ASV abundance table (McMurdie and Holmes 2014). The fold-change in abundance of each ASV was calculated using the R package "DESeq2" v1.16.1 (Love et al. 2014). The method applies a generalized exact binomial test on variance stabilized ASV abundance. The results were filtered by significance, after correction for multiple-testing according to Benjamini and Hochberg (1995) with an adjusted p value < 0.1.

In other locations sampled during PS107, bacterioplankton communities were collected without size fractionation and sequenced separately using the same protocol as described above. In order to compare the communities of the submesoscale filament to these other Fram Strait locations, we agglomerated the sequences of free-living and particle-associated communities. Due to these methodological discrepancies, comparison between the communities was conducted on genus level as the lowest mutual taxonomic rank.

Data accession numbers and analyses repository

Raw paired-end, primer-trimmed reads were deposited in the European Nucleotide Archive (ENA; Silvester et al. 2018) under project accession number: PRJEB34666. The data were archived using the brokerage service of the German Federation for Biological Data (GFBio; Diepenbroek et al. 2014). Scripts for processing data can be accessed at "https://github.com/edfadeev/submesoscale_analysis."

Results

General characteristics of the submesoscale filament

In late July 2017, sea ice was present in the Fram Strait northeast and west of 0°EW/80°N (>15% concentration) while the eastern part of the Fram Strait was ice-free (Fig. 1a). On 26th of July 2017, satellite radar reflectivity showed a nearly straight streak of sea ice in the marginal ice zone at 2.5°E/79°N, which extended over 50 km from northeast to southwest and had a width of only 500 m (Fig. 1b). Below this sea-ice streak, we found a ca. 8 km wide filament characterized

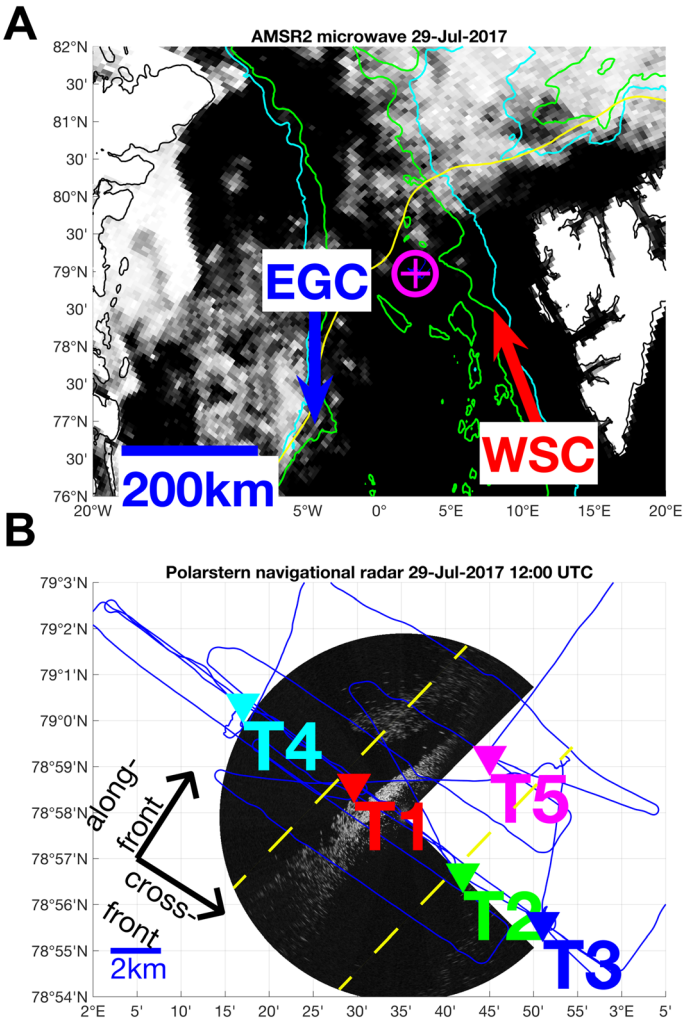

Fig 1. Geographic location and sampling scheme of the submesoscale filament. (**a**) Sea ice distribution in the study area (black = open water, white = sea ice) based on AMSR2 microwave data from 29 July 2017. The magenta plus marks the filament location. (**b**) RV Polarstern navigational radar reflectivity on 29 July 2017 12:00 UTC approaching the ice streak. The blue line shows the cruise track. Colored triangles mark the CTD stations: T1 (red), T2 (green), T3 (blue), T4 (cyan), and T5 (magenta). The filament was located approximately between the yellow dashed lines. Adapted from von Appen et al. (2018).

by a thin surface meltwater layer, above a layer of denser water that extended to >250 m depth.

Based on defined temperature and salinity characteristics of the main water masses in the Fram Strait (Rudels et al. 2013), both Atlantic water (temperature maximum > 5°C) and Polar water (temperature minima of ca. −1°C) were observed (Fig. 2). Outside of the filament, the surface ocean was strongly stratified by meltwater that occupied the top 15 m of the water column. Polar water was located directly below the meltwater layer at 20–40 m depth, while Atlantic water extended below the Polar water between 50 and 250 m depth. By contrast, inside the filament the meltwater layer covered

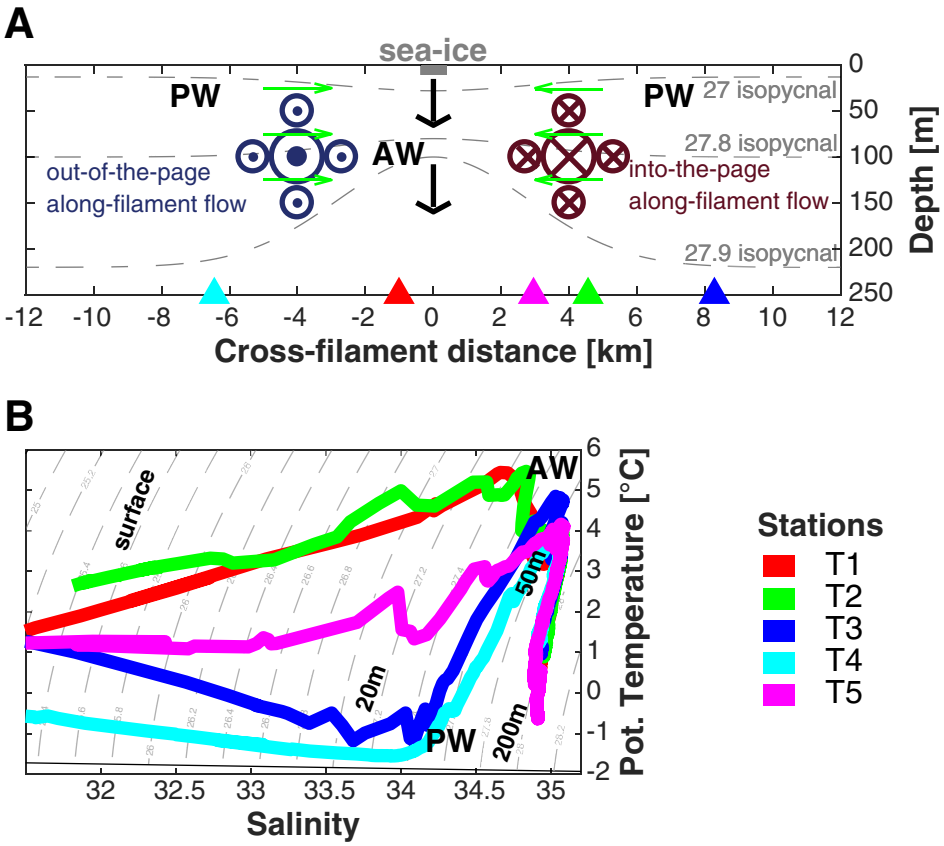

Fig 2. Schematic section of the submesoscale filament and its water mass characteristics. (**a**) Representation of the physical processes inside the filament determined from underway CTD profiles at 800 m resolution. Below ~ 50 m depth isopycnals (lines of constant density) of the Atlantic water (AW) are raised in the centre of the filament, while isopycnals of the polar water (PW) are depressed at shallower depth. The depressed isopycnals in the centre are associated with subduction and the accumulation of sea ice. The horizontal flow is parallel to the filament (into-/out-of-the-page) as well as convergent towards the centre of the filament. The colored triangles represent the different sampling station, according to the legend. (**b**) Temperature-salinity diagram of the CTD profile at each sampling station, and the Atlantic water (AW) and polar water (PW) characteristics. Adapted from von Appen et al. (2018).

the top 25 m, below which a relatively shallower and denser Atlantic water layer (25–250 m) was found (Fig. 2). High-resolution physical characterization revealed a frontal system of two strong currents flowing in opposite directions along the filament (Fig. 2a). These currents led to a horizontal inward-flow from both sides and mixing mostly in the upper 100 m inside the filament, apparent in the temperature and salinity characteristics of station T5 (Fig. 2b). Furthermore, von Appen et al. (2018) suggested that the denser waters (27.9 kg m^{-3}) at ca. 100 m depth inside the filament were in the process of subduction, with an estimated vertical velocity of up to 100 m d^{-1} (Fig. 2a). Together, these mixing processes apparently enhanced phytoplankton growth in the filament waters, most likely by providing nutrients.

Biogeochemical conditions in the filament and the bounding currents

For biogeochemical and molecular analyses, water samples were collected inside the filament at stations T1, T2, and station T5 where strong mixing between Atlantic and Polar waters was observed (Fig. 2). Water samples from stations T3 and T4 represented the bounding currents on either side of the filament (Fig. 2). At each station, water samples were collected at six representative layers: surface (10 m), chlorophyll *a* maximum (chl-*a* max.; 20–30 m), below chl-*a* max. (50 m), epipelagic (100 m), and mesopelagic (200 and 400 m).

The ice melt-influenced surface waters inside the filament (measured at 10 m) were strongly depleted in nitrate (NO_3), with $(NO_3 + NH_4)/PO_4$ ratios of 2.2–3.3, compared to 5.5–11.8 outside of the filament (Table 1). Partial pressure of carbon dioxide (pCO_2) in surface waters inside the filament was below 250 µatm, compared to ca. 300 µatm outside of the filament, recording the enhanced primary production. At the chl-*a* max. Depth (20–30 m), chl-*a* inside the filament ranged from 0.6 to 2.9 mg m^{-3}, peaking at station T5 (Table 1). In contrast, outside of the filament chl-*a* showed intermediate concentrations at the south-eastern station T3 (0.6–0.9 mg m^{-3}), and low concentrations at the north-

Table 1. Overview of biogeochemical parameters and phytoplankton biomass at all sampled stations

Station	Lat. (°N)/ long. (°E)	Depth (m)	NO_3 (µmol L^{-1})	NH_4 (µmol L^{-1})	PO_4^{3-} (µmol L^{-1})	$(NO_3 + NH_4)$/ PO_4 ratio	$Si(OH)_3$ (µmol L^{-1})	PbSi (µmol L^{-1})	Chl- *a* (mg m^{-3})	POC (µg L^{-1})	Centric diatoms ($\times 10^3$ cells mL^{-1})	Pennate diatoms ($\times 10^3$ cells mL^{-1})	Diatom PPC* (µg L^{-1})	*Phaeocystis* spp. ($\times 10^3$ cells mL^{-1})	*Phaeocystis* PPC (µg L^{-1})	Bacterioplankton ($\times 10^5$ cells mL^{-1})
T1*	78.98/2.49	10	0.03	0.26	0.13	2.2	2.4	1.1	0.6	235.7	4.5	6.5	72	13	55	2.7
		20	0.07	–	0.17	2.4	2.3	1.1	2.2	407.3	7.8	11.6	189	18.4	55	5.9
		50	3.43	1.98	0.44	12.3	3.6	–	0.2	121	–	–	–	–	–	9.7
T2*	78.94/2.70	10	0.06	0.17	0.09	2.6	1.7	1	0.9	289.6	5.8	8.3	188	17.6	35	3.6
		30	3.95	1.26	0.34	15.3	3.6	0.5	0.9	147.8	6	4.2	56	7.8	16	11
		50	7.2	1.48	0.54	16.1	3.8	0.1	0.2	96.4	–	–	–	–	–	7.3
T3	78.93/2.85	10	1.37	0.17	0.28	5.5	4.2	0.9	0.9	225.8	8.9	6.2	101	14.5	29	4.3
		30	7.05	0.43	0.54	13.9	3.7	0.1	0.6	107.2	9.6	3.6	50	12.7	25	4.9
		50	12.19	0.35	0.73	17.2	4.3	0.1	0.1	64.3	–	–	–	–	–	3.2
T4	79.01/2.28	10	6.39	0.2	0.56	11.8	5.4	0.1	0.3	52.1	–	–	–	–	–	2.2
		30	7.88	0.22	0.58	14.0	3.8	0.1	0.2	31.2	–	–	–	–	–	2
		50	9.09	0.39	0.63	15.0	4.7	–	0.1	30.1	–	–	–	–	–	1.9
T5*	78.99/2.76	10	0.14	0.51	0.2	3.3	2.2	1.6	2	286.3	13.6	9.7	172	35.9	72	4.4
		25	3.85	0.43	0.36	11.9	2.8	0.9	2.9	221.3	3.4	12.9	156	26.7	53	6.4
		50	8.89	0.78	0.64	15.1	3.6	0.1	0.1	57.4	–	–	–	–	–	4.4

PPC, phytoplankton carbon content; –, No available data.
*Stations inside the submesoscale filament.

western station T4 (<0.3 mg m^{-3}). Furthermore, in the upper 30 m, the POC concentrations and cell abundances of *Phaeocystis*—a major phytoplankton group—were also ca. twofold higher inside compared to outside of the filament (Table 1).

We deployed free-drifting sediment traps to quantify particulate organic carbon (POC) flux to 100, 200 and 400 m depth, both inside (near station T1), and outside (near the southeastern station T3) of the filament (Table 2). Both inside and outside the filament, we observed a similar POC flux of 50 and 55 mgPOC m^{-2} d^{-1} to 100 m, respectively (Table 2). However, the POC flux to 200 and 400 m depth inside the filament was almost twofold larger (48–56 mgPOC m^{-2} d^{-1}) compared to outside of the filament (28–37 mgPOC m^{-2} d^{-1}). This supports the hypothesis of von Appen et al. (2018) of a substantial subduction inside the filament, speeding up the transport of particles from the mixed upper 100 m to higher depths.

Abundance and diversity of bacterioplankton communities in the filament and the bounding currents

Bacterioplankton cell abundances correlated with chl-*a* concentrations (Spearman's rank correlation, $r_s = 0.8$, $p < 0.001$). Inside the filament bacterioplankton cell abundances reached up to 1.1×10^6 cells mL^{-1} (station T5), compared to twofold lower abundances outside of the filament, with well below 0.5×10^6 cells mL^{-1} (Table 1). Beneath the upper 50 m, no differences in total cell abundances were observed (Supporting information Table S2). At all stations and sampling depths, we characterized the free-living (FL) and the particle-associated (PA) bacterioplankton communities using 16S rRNA gene amplicon sequencing. The final dataset consisted of 5,770,041 sequences in 59 samples that were assigned to 3980 amplicon sequence variants (ASVs; Supporting information Table S1). Rarefaction curves did not reach a plateau in any of the sampled communities, however, estimated asymptotic extrapolation to double amount of sequences showed only few additional ASVs (Supporting information Fig. 1). Thus, our sequencing depth represented most of the bacterioplankton diversity (Hsieh et al., 2016). Overall, bacterioplankton inside and outside of the filament was dominated by typical seawater taxonomic groups, i.e., the classes *Alphaproteobacteria*, *Bacteroidia*, and *Gammaproteobacteria* (Supporting information Fig. 2). Furthermore, surface water (10 m depth) communities outside of the filament had higher similarity to bacterioplankton communities in the western Fram Strait (i.e., Polar water; Supporting information Fig. 3). On the other hand, communities inside the filament had higher similarity to bacterioplankton communities in the eastern and northern parts of the Fram Strait (i.e., Atlantic water; Supporting information Fig. 3).

Alpha-diversity estimators of both free-living and particle-associated bacterioplankton revealed ca. twofold higher community richness in the epipelagic and mesopelagic depths (>100 m), compared to the upper 50 m (*t*-test, $p < 0.05$;

Table 2. Vertical fluxes of POC measured using free-drifting sediment traps.

	Deployment		Recovery			
Station	**Date**	**Lat. (°N)/long. (°E)**	**Date**	**Lat. (°N)/long. (°E)**	**Depth (m)**	**POC flux* (mgPOC m^{-2} d^{-1})**
T1	29 July 2017	78.97/2.49	30 July 2017	78.98/2.88	100	50 ± 2.7
					200	48 ± 2.5
					400	56 ± 3.0
T3	30July 2017	78.92/2.86	31 July 2017	79.14/3.19	100	56 ± 3.0
					200	28 ± 1.5
					400	37 ± 2.0

*The standard deviation for the POC flux was estimated as a conservative technical error based on the data provided for deviation for the aliquots for the wet splitting of the samples (<5.0%) and the precision for the EuroEA Elemental Analyzer (±0.3%), resulting in a 5.3% error.

Supporting information Table 1). Furthermore, in the upper 50 m inside the filament, the number of observed ASVs and the Chao1 richness were lower (*t*-test, $p < 0.05$; Supporting information Fig. 4). Below the upper 50 m, there were no significant differences between bacterioplankton alpha diversity inside and outside the filament (*t*-test, $p > 0.05$; Supporting information Fig. 4).

The composition of bacterioplankton communities showed a separation of the free-living and particle-associated communities at all depths (PERMANOVA, $R^2 = 0.22$, $p < 0.001$; Supporting information Fig. 5). In both fractions there was a clear separation between the communities in the upper 50 m and below (PERMANOVA, $R^2 = 0.16$, $p < 0.001$). In the upper 50 m (surface, chl-*a* max. and below chl-*a* max.), where most of the biogeochemical variability was observed, the composition of the bacterioplankton communities significantly differed inside and outside of the submesoscale filament (PERMANOVA, $R^2 = 0.13$, $p < 0.001$; Fig. 3). However, the surface (10 m) bacterioplankton community at station T3 (outside of the filament) showed compositional similarity to the respective communities inside the filament (Fig. 3). In contrast, in the Atlantic water masses below the upper 50 m (lower epipelagic and mesopelagic communities), there was no significant difference between the composition of the bacterioplankton communities inside and outside of the filament (PERMANOVA, $p > 0.05$; Supporting information Fig. 5).

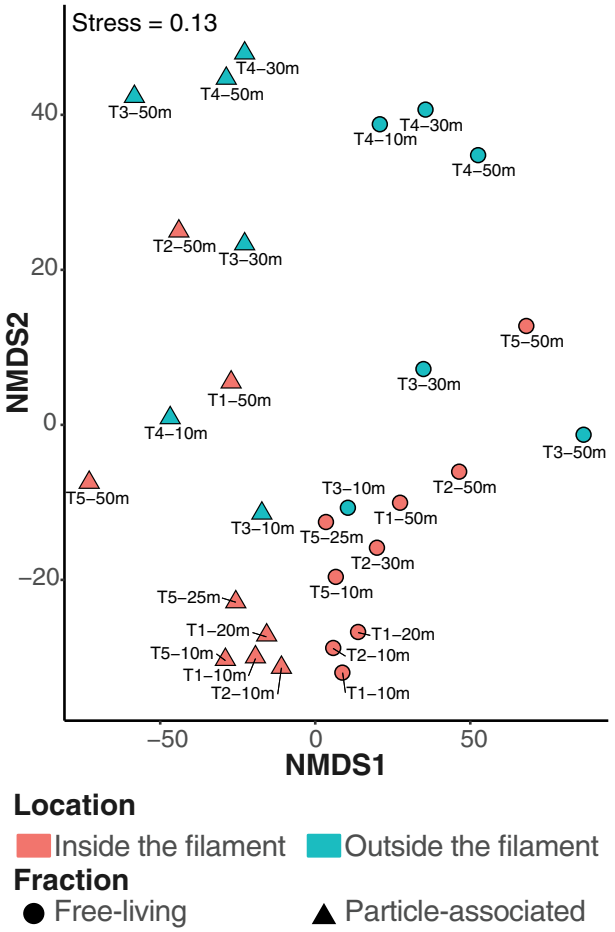

Fig 3. Nonmetric multidimensional scaling of free-living and particle-associated communities in the upper 50 m. Communities inside and outside of the filament are colored in red and blue, respectively. Stars represent the centroid of the communities inside and outside of the filament. Circles represent free-living and triangles particle-associated communities, respectively. The labels consist of the sampling station and an abbreviation of the sampling depth: S—surface (10 m), C—chl-*a* max. (20–30 m), B—below chl-*a* max. (50 m).

Taxonomic composition of bacterioplankton communities

To investigate which taxonomic lineages accounted for the observed community differences, we performed an ASV presence/absence analysis. We revealed that 727 ASVs (18% of total ASVs) were shared among all free-living and particle-associated communities (Fig. 4). These shared ASVs constituted ca. 90% of all bacterioplankton sequences in the upper 50 m and below, and were mainly associated with the order *Flavobacteriales* (*Bacteroidia*; 112 ASVs) and the SAR11 clade (*Alphaproteobacteria*; 95 ASVs). In addition, 265 ASVs, also mainly associated with *Flavobacteriales* and the SAR11 clade, were unique to the upper 50 m bacterioplankton communities

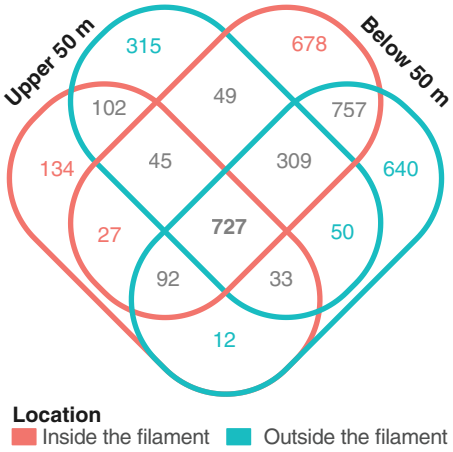

Fig 4. Venn diagram of shared and unique ASVs between bacterioplankton communities. Communities inside and outside of the filament are colored in red and blue, respectively.

inside the filament. On the other hand, 723 ASVs were unique to the upper 50 m bacterioplankton communities outside of the filament, and were mainly associated with the clades SAR11, SAR202, and SAR406. These unique ASVs comprised ca. 1% and 2% of the bacterioplankton sequences inside and outside of the filament, respectively. Below the upper 50 m, a similar amount of unique ASVs were observed inside and outside the filament (799 and 735 ASVs, respectively), mostly associated with *Flavobacteriales* and the clades SAR11, SAR406 and SAR202.

We further investigated the differential sequence abundance of the shared ASVs in both free-living and particle-associated communities of the upper 50 m inside and outside of the filament (Fig. 5). The ASVs associated with *Flavobacteriales* (mainly families *Flavobacteriaceae* and *Cryomorphaceae*) and the SAR11 clade (mainly ecotype I and II) were significantly enriched inside the filament (Supporting information Table 3) and comprising 23%–56% of the sequences, in contrast to 6%–28% outside of the filament (Supporting information Fig. 6). Outside the filament, the communities were significantly enriched in various taxonomic groups, including the SAR202 clade and the archaeal order *Nitrosopumilales* (Supporting information Table 3), which comprised 3%–21% of the sequences in bacterioplankton communities outside of the filament compared to <3% inside the filament.

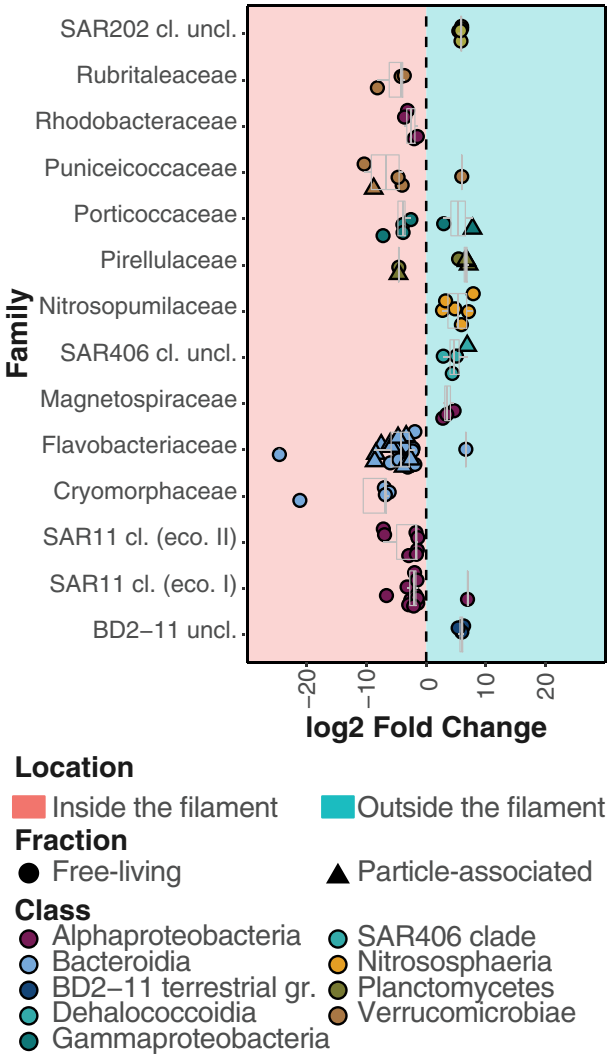

Fig 5. Differential enrichment analysis comparing ASV abundances inside (left red panel) and outside (right blue panel) of the submesoscale filament. The x-axis represents the $\log_2$ fold change for all ASVs within each family. The boxplots represent the mean and the standard deviation of ASVs $\log_2$ fold change in each taxonomic family. Positive and negative values represent enrichment outside and inside of the filament, respectively. Different taxonomic classes are represented by color code. Circles represent free-living and triangles particle-associated communities, respectively. Only families with at least two significantly enriched (adjusted $p < 0.1$) ASVs were included in the figure. (uncl): Classified on higher taxonomic level.

Discussion

Previous observations of low-latitude frontal systems revealed that they trigger phytoplankton growth (Taylor et al. 2012; Clayton et al. 2014; von Appen et al. 2020). In this study, we conducted the first biogeochemical and molecular characterization of an Arctic surface submesoscale frontal filament, observed in the Fram Strait (von Appen et al. 2018). The distinct biogeochemical differences in the upper 30 m inside and outside of the filament were a result of locally enhanced primary production, enabled by horizontal mixing between nutrient-rich Atlantic and nutrient-depleted Polar waters. The $(NO_3 + NH_4)/PO_4$ ratio indicated nitrate depletion by ongoing phytoplankton growth in the filament, and at its south-eastern edge (station T3). The chl-*a* and POC concentrations, as well as phytoplankton cell abundances, were more than twofold higher inside the filament. The observed chl-*a*

concentrations (up to 2.9 mg m^{-3}) inside the filament were also relatively high in comparison to typically observed 1–2 mg m^{-3} during seasonal phytoplankton blooms in the region (Nöthig et al. 2015; Fadeev et al. 2018; Randelhoff et al. 2018). Combined with the enhanced drawdown of pCO_2, nitrate depletion and the overall higher export flux, our evidence indicate a substantial stimulation of phytoplankton growth and export associated with the filament. These observations support the hypothesis that phytoplankton of high-latitudes may rapidly exploit submesoscale processes and produce substantial biomass, especially when nutrient-rich water masses are mixed by fronts such as the one observed here (Boyd et al. 2000; Taylor and Ferrari 2011; Lévy et al. 2012, 2018).

Despite the twofold higher concentrations of chl-*a*, POC, and phytoplankton inside the filament compared to its surrounding waters, we observed a similar flux of ca. 50 mgPOC m^{-2} d^{-1} to 100 m depth (i.e., the uppermost sediment trap) both inside and outside of the filament. This POC flux corresponded to previous measurements during seasonal phytoplankton blooms in the Fram Strait (Lalande et al. 2013; Fadeev et al. 2020), and suggested an export of fresh POC from the top meltwater layer inside and outside the filament at the time of sampling. A potential explanation for this pattern is the higher primary production in the deeper surface layer inside the filament, and the stronger mixing rate in the Atlantic water layer below. Previous observations in the region showed that particle sinking velocities are 20–60 m d^{-1}, and that there are faster sinking particles in ice-associated conditions (Fadeev et al. 2020). Therefore, it is likely that the POC formed at the surface inside the filament was then more rapidly exported to depths > 100 m by higher sinking rates and by physical water subduction. Furthermore, a time lag between production rates and export to deep waters cannot be excluded. In any case, the observed submesoscale process increased the export efficiency resulting in twofold larger POC export to depths below 100 m in the filament compared to the surrounding waters.

During the summer, surface waters bacterioplankton communities are mostly shaped by seasonal phytoplankton bloom conditions, with only small diversity variation between Atlantic and Polar water masses (Wilson et al. 2017; Fadeev et al. 2018). The response of bacterioplankton communities to blooming phytoplankton is often associated with elevated cell abundances and a change in taxonomic composition (Bunse and Pinhassi 2017). In the upper 50 m inside the filament, we observed higher bacterioplankton cell abundances and lower diversity of the communities, indicating the stimulation of specific taxonomic groups. The bacterioplankton communities inside the filament were enriched (in terms of sequence abundance) by ASVs of the order *Flavobacteriales* (class *Bacteroidia*), which specializes on degrading phytoplankton-derived organic compounds (Teeling et al. 2012) and is typically found during phytoplankton blooms (Buchan et al. 2014; Teeling et al. 2016). Furthermore, surface bacterioplankton communities inside the filament showed higher compositional similarity to communities sampled during the same cruise in Atlantic water of the West Spitsbergen Current, where elevated chl-*a* values indicated phytoplankton growth (Liu et al. 2019). In comparison, the upper 50 m bacterioplankton communities outside of the filament had lower cell abundances combined with higher taxonomic diversity. These communities were enriched in ASVs from SAR406 (phylum *Marinimicrobia*), SAR202 (class *Dehalococcoidia*), and the archaeal order *Nitrosopumilales*. Thus, surface bacterioplankton communities outside the filament resembled the communities in the Polar water of the East Greenland Current, where chl-*a* values did not show a pronounced phytoplankton growth (Liu et al. 2019). Taken together, our results suggest that overall composition of the bacterioplankton communities in the filament reflected both the origin of the water mass (mainly observed in the presence/absence of taxa), and a response to the enhanced phytoplankton growth. Combined with the strongly depleted nitrate, the higher ammonia concentrations (Table 1) and the overall enhanced export flux, we further speculate that there was already an elevated heterotrophic microbial activity inside the filament as typical for the later bloom stage (Piontek et al. 2014; Fadeev et al. 2018).

The total "lifetime" of the observed submesoscale filament is unknown. Taking into account lateral advection velocities of ca. 10 cm s^{-1} (Wekerle et al. 2017) and the observed pronounced biological signal, the scenario of the filament being a result of a lateral transport from a remote phytoplankton bloom is unlikely. Based on the assumption that physicochemical-biological dynamics originate from localized temporal evolution, rather than advected biomass, the age of the filament at the time of sampling can be estimated from changes in microbial cell abundances. With phytoplankton doubling times of 2–3 d at 4–6°C water temperatures (Kremer et al., 2017), reaching up to threefold higher cell abundances inside the filament would require up to 9 d. This temporal scale is consistent with the time required to reach the twofold higher cell abundances inside the filament (doubling time every 10 d; Kirchman et al. 2009). These growth-rate estimates do not take into account potential losses due to grazing by zooplankton or viral lysis, and thus represent rather the lower time limit. Based on this we hypothesize that, at the time of sampling, the age of the observed filament was already at least 10 d. Although temporal dynamics are not resolved by our sampling strategy, the approximated lifetime matches recent estimates of mesoscale eddies lifetime in Fram Strait based on high-resolution ocean-sea ice models (Wekerle et al. 2020). The boundaries of these mesoscale eddies may harbor submesoscale filaments such as the one studied here.

In conclusion, we showed that the mixing between Atlantic and Polar waters formed a spatially restricted water filament with distinct biological and biogeochemical characteristics. Its presumed persistence for at least 10 d is projected to have direct implications for organic matter export, to

some extent enhanced via vertical subduction. We also showed that higher phytoplankton biomass inside the filament was associated with a pronounced change in the abundance and composition of bacterioplankton communities, towards dominance of heterotrophic "master recyclers." Taken together, our observations support the hypothesis that submesoscale features with sizes from kilometers to tens of kilometers promote phytoplankton blooms by nutrient supply (Lévy et al. 2001; Mouriño 2004; Mahadevan 2015), and that these features directly shape microbial diversity and community structure on small spatial and temporal scales (Lévy et al. 2012, 2018). Altogether, corresponding to estimates of the regularity of such phenomena in the ocean (Lévy et al. 2018), our observations support the notion that submesoscale processes play an important role in ocean productivity, biogeochemical fluxes and biodiversity patterns.

Most submesoscale filaments and previously studied frontal systems result from temperature gradients between two semi-stationary water masses (e.g., Baltar et al. 2009, 2016). The Arctic submesoscale filament observed here is the result of the strong salinity gradient between Atlantic and Polar waters. To produce similar density gradients, water masses would have to have temperature differences of several tens of °C, which does not occur in the studied Arctic region. However, such strong salinity gradients can be found not only in the Fram Strait, but also in other ice- or freshwater-influenced regions worldwide, such as estuarine systems (Jaeger and Mahadevan 2018). Despite the fundamental nonphysical differences between such environments, similar physical submesoscale dynamics driven by the density gradients are to be expected. We therefore suggest that similar pronounced localized biological responses to physical processes as well as physical–biological interactions may also occur in other aquatic systems. To assess their impact on regional and global ocean productivity, high resolution methods would be needed, such as long range autonomous underwater vehicles or towed vehicles in combination with remote sensing by satellite. However, especially in polar regions, the ice cover limits quantification by remote sensing, challenging to understand and predict how the regional productivity is impacted by such submesoscale processes. This study provides a combination of methods that improves such predictions.

References

Azam, F., and F. Malfatti. 2007. Microbial structuring of marine ecosystems. Nat. Rev. Microbiol. **5**: 782–791. doi:10.1038/nrmicro1747

Baltar, F., and J. Arístegui. 2017. Fronts at the Surface Ocean can shape distinct regions of microbial activity and community assemblages down to the bathypelagic zone: The Azores front as a case study. Front. Mar. Sci. **4**: 1–13. doi:10.3389/fmars.2017.00252

Baltar, F., J. Arístegui, J. Gasol, S. Hernández-León, and G. Herndl. 2007. Strong coast-ocean and surface-depth gradients in prokaryotic assemblage structure and activity in a coastal transition zone region. Aquat. Microb. Ecol. **50**: 63–74. doi:10.3354/ame01156

Baltar, F., J. Arístegui, M. F. Montero, M. Espino, J. M. Gasol, and G. J. Herndl. 2009. Mesoscale variability modulates seasonal changes in the trophic structure of nano- and picoplankton communities across the NW Africa-Canary Islands transition zone. Prog. Oceanogr. **83**: 180–188. doi:10.1016/j.pocean.2009.07.016

Baltar, F., J. Arístegui, J. M. Gasol, I. Lekunberri, and G. J. Herndl. 2010. Mesoscale eddies: Hotspots of prokaryotic activity and differential community structure in the ocean. ISME J. **4**: 975–988. doi:10.1038/ismej.2010.33

Baltar, F., K. Currie, E. Stuck, S. Roosa, and S. E. Morales. 2016. Oceanic fronts: Transition zones for bacterioplankton community composition. Environ. Microbiol. Rep. **8**: 132–138. doi:10.1111/1758-2229.12362

Benjamini, Y., and Y. Hochberg. 1995. Controlling the false discovery rate: A practical and powerful approach to multiple testing. J. R. Stat. Soc. Ser. B **57**: 289–300. doi:https://doi.org/10.1111/j.2517-6161.1995.tb02031.x

Beszczynska-Möller, A., E. Fahrbach, U. Schauer, E. Hansen, A. Beszczynska-Moller, E. Fahrbach, U. Schauer, and E. Hansen. 2012. Variability in Atlantic water temperature and transport at the entrance to the Arctic Ocean, 1997-2010. ICES J. Mar. Sci. **69**: 852–863. doi:10.1093/icesjms/fss056

Boyd, P. W., A. J. Watson, C. S. Law, and others. 2000. A mesoscale phytoplankton bloom in the polar Southern Ocean stimulated by iron fertilization. Nature **407**: 695–702. doi:10.1038/35037500

Buchan, A., G. R. LeCleir, C. A. Gulvik, J. M. González, and J. M. Gonzalez. 2014. Master recyclers: Features and functions of bacteria associated with phytoplankton blooms. Nat. Rev. Microbiol. **12**: 686–698. doi:10.1038/nrmicro3326

Bunse, C., and J. Pinhassi. 2017. Marine Bacterioplankton seasonal succession dynamics. Trends Microbiol. **25**: 494–505. doi:10.1016/j.tim.2016.12.013

Callahan, B. J., P. J. McMurdie, M. J. Rosen, A. W. Han, A. J. A. Johnson, and S. P. Holmes. 2016. DADA2: High-resolution sample inference from Illumina amplicon data. Nat. Methods **13**: 581–583. doi:10.1038/nmeth.3869

Clayton, S., T. Nagai, and M. J. Follows. 2014. Fine scale phytoplankton community structure across the Kuroshio front. J. Plankton Res. **36**: 1017–1030. doi:10.1093/plankt/fbu020

de Steur, L., E. Hansen, R. Gerdes, M. Karcher, E. Fahrbach, and J. Holfort. 2009. Freshwater fluxes in the East Greenland current: A decade of observations. Geophys. Res. Lett. **36**: L23611. doi:10.1029/2009GL041278

Diepenbroek, M., F. O. Glöckner, P. Grobe, and others. 2014. Towards an integrated biodiversity and ecological research data management and archiving platform: The German

federation for the curation of biological data (GFBio). Informatik 2014: 1711–1721. Gesellschaft für Informatik e.V. https://dl.gi.de/handle/20.500.12116/2782

Djurhuus, A., P. H. Boersch-Supan, S.-O. Mikalsen, and A. D. Rogers. 2017. Microbe biogeography tracks water masses in a dynamic oceanic frontal system. R. Soc. Open Sci. **4**: 170033. doi:10.1098/rsos.170033

Dusa, A. 2020. venn: Draw Venn Diagrams. https://CRAN.R-project.org/package=venn

Edler, L. 1979. Recommendations on methods for marine biological studies in the Baltic Sea. Phytoplankton and chlorophyll. *In* Baltic Marine Biologists. **5**: 1–38.

Evans, C. A., and S. E. O'Reilly. 1982. A manual for measurement of chlorophyll a, net phytoplankton and nanoplankton. BIOMASS Handb. Ser, BIOMASS.

Fadeev, E., I. Salter, V. Schourup-Kristensen, and others. 2018. Microbial communities in the east and west Fram Strait during sea ice melting season. Front. Mar. Sci. **5**: 429. doi:10.3389/fmars.2018.00429

Fadeev, E., A. Rogge, S. Ramondenc, and others. 2020. Sea-ice retreat may decrease carbon export and vertical microbial connectivity in the Eurasian Arctic basins. Nat. Res. doi:10.21203/rs.3.rs-101878/v1

Ferrari, R. 2011. A frontal challenge for climate models. Science (80-.) **332**: 316–317. doi:10.1126/science.1203632

Fuhrman, J. A., I. Hewson, M. S. Schwalbach, J. A. Steele, M. V. Brown, and S. Naeem. 2006. Annually reoccurring bacterial communities are predictable from ocean conditions. Proc. Natl. Acad. Sci. U. S. A. **103**: 13104–13109. doi:10.1073/pnas.0602399103

Gasol, J. M., and P. A. Del Giorgio. 2000. Using flow cytometry for counting natural planktonic bacteria and understanding the structure of planktonic bacterial communities. Sci. Mar. **64**: 197–224. doi:10.3989/scimar.2000.64n2197

Gómez-Rubio, V. 2017. ggplot2 - elegant graphics for data analysis (2nd Edition). J. Stat. Softw **77**: (Book Review 2) http://dx.doi.org/10.18637/jss.v077.b02

Grasshoff, K., K. Kremling, and M. Ehrhardt. 2009. Methods of seawater analysis. John Wiley & Sons.

Hsieh, T. C., K. H. Ma, and A. Chao. 2016. iNEXT: An R package for rarefaction and extrapolation of species diversity (hill numbers). Methods Ecol. Evol. **7**: 1451–1456. doi:10.1111/2041-210X.12613

Jaeger, G. S., and A. Mahadevan. 2018. Submesoscale-selective compensation of fronts in a salinity-stratified ocean. Sci. Adv. **4**: 1–10. doi:10.1126/sciadv.1701504

Kérouel, R., and A. Aminot. 1997. Fluorometric determination of ammonia in sea and estuarine waters by direct segmented flow analysis. Mar. Chem. **57**: 265–275. doi:10.1016/S0304-4203(97)00040-6

Kirchman, D. L., X. A. G. Morán, and H. Ducklow. 2009. Microbial growth in the polar oceans: Role of temperature and potential impact of climate change. Nat. Rev. Microbiol. **7**: 451–459. doi:10.1038/nrmicro2115

Kremer, C. T., M. K. Thomas, and E. Litchman. 2017. Temperature- and size-scaling of phytoplankton population growth rates: Reconciling the Eppley curve and the metabolic theory of ecology. Limnol. Oceanogr. **62**: 1658–1670. doi:10.1002/lno.10523

Lalande, C., E. Bauerfeind, E. Nöthig, and A. Beszczynska-Möller. 2013. Impact of a warm anomaly on export fluxes of biogenic matter in the eastern Fram Strait. Prog. Oceanogr. **109**: 70–77. doi:10.1016/j.pocean.2012.09.006

Lévy, M., P. Klein, and A.-M. Treguier. 2001. Impact of sub-mesoscale physics on production and subduction of phytoplankton in an oligotrophic regime. J. Mar. Res. **59**: 535–565. doi:10.1357/002224001762842181

Lévy, M., R. Ferrari, P. J. S. Franks, A. P. Martin, and P. Rivière. 2012. Bringing physics to life at the submesoscale. Geophys. Res. Lett. **39**: 1–13. doi:10.1029/2012GL052756

Lévy, M., P. J. S. Franks, and K. S. Smith. 2018. The role of submesoscale currents in structuring marine ecosystems. Nat. Commun. **9**: 4758. doi:10.1038/s41467-018-07059-3

Liu, Y., E. Boss, A. Chase, H. Xi, X. Zhang, R. Röttgers, Y. Pan, and A. Bracher. 2019. Retrieval of phytoplankton pigments from underway spectrophotometry in the Fram Strait. Remote Sens. (Basel) **11**: 318. doi:10.3390/rs11030318

Love, M. I., W. Huber, and S. Anders. 2014. Moderated estimation of fold change and dispersion for RNA-seq data with DESeq2. Genome Biol. **15**: 550. doi:10.1186/s13059-014-0550-8

Mahadevan, A. 2015. The impact of submesoscale physics on primary productivity of plankton. Ann. Rev. Mar. Sci. **8**: 161–184. doi:10.1146/annurev-marine-010814-015912

Martin, M. 2011. Cutadapt removes adapter sequences from high-throughput sequencing reads. EMBnet J **17**: 10. doi:10.14806/ej.17.1.200

McMurdie, P. J., and S. Holmes. 2013. Phyloseq: An R package for reproducible interactive analysis and graphics of microbiome census data M. Watson [ed.]. PLoS One **8**: e61217. doi:10.1371/journal.pone.0061217

McMurdie, P. J., and S. Holmes. 2014. Waste not, want not: why rarefying microbiome data is inadmissible. PLoS Comput. Biol. **10**: e1003531. doi:10.1371/journal.pcbi.1003531

McWilliams, J. C. 2016. Submesoscale currents in the ocean. Proc. R. Soc. A Math. Phys. Eng. Sci **472**: 20160117. doi:10.1098/rspa.2016.0117

Mouriño, B. 2004. Thermohaline structure, ageostrophic vertical velocity fields and phytoplankton distribution and production in the Northeast Atlantic subtropical front. J. Geophys. Res. **109**: C04020. doi:10.1029/2003JC001990

Müller, O., B. Wilson, M. L. Paulsen, A. Rumińska, H. R. Armo, G. Bratbak, and L. Øvreås. 2018. Spatiotemporal dynamics of ammonia-oxidizing thaumarchaeota in distinct Arctic water masses. Front. Microbiol. **9**: 1–13. doi:10.3389/fmicb.2018.00024

Nelson, C. E., C. A. Carlson, C. S. Ewart, and E. R. Halewood. 2014. Community differentiation and population

enrichment of Sargasso Sea bacterioplankton in the euphotic zone of a mesoscale mode-water eddy. Environ. Microbiol. **16**: 871–887. doi:10.1111/1462-2920.12241

Nöthig, E. M., A. Bracher, A. Engel, and others. 2015. Summertime plankton ecology in fram strait-a compilation of long- and short-term observations. Polar Res. **34**: 23349. doi:10.3402/polar.v34.23349

Oksanen, J., F. G. Blanchet, M. Friendly, and others. 2019. vegan: Community Ecology Package. https://CRAN.R-project.org/package=vegan

Parada, A. E., D. M. Needham, and J. A. Fuhrman. 2016. Every base matters: Assessing small subunit rRNA primers for marine microbiomes with mock communities, time series and global field samples. Environ. Microbiol. **18**: 1403–1414. doi:10.1111/1462-2920.13023

Piontek, J., M. Sperling, E.-M. Nöthig, and A. Engel. 2014. Regulation of bacterioplankton activity in Fram Strait (Arctic Ocean) during early summer: The role of organic matter supply and temperature. J. Mar. Syst. **132**: 83–94. doi:10.1016/j.jmarsys.2014.01.003

Quast, C., E. Pruesse, P. Yilmaz, J. Gerken, T. Schweer, F. O. Glo, and P. Yarza. 2013. The SILVA ribosomal RNA gene database project: Improved data processing and web-based tools. **41**: D590–D596. doi:10.1093/nar/gks1219

Randelhoff, A., M. Reigstad, M. Chierici, and others. 2018. Seasonality of the physical and biogeochemical hydrography in the inflow to the Arctic Ocean through Fram Strait. Front. Mar. Sci. **5**: 224. doi:10.3389/fmars.2018.00224

Rudels, B., U. Schauer, G. Björk, M. Korhonen, S. Pisarev, B. Rabe, and A. Wisotzki. 2013. Observations of water masses and circulation with focus on the Eurasian Basin of the Arctic Ocean from the 1990s to the late 2000s. Ocean Sci. **9**: 147–169. doi:10.5194/os-9-147-2013

Sasaki, H., P. Klein, B. Qiu, and Y. Sasai. 2014. Impact of oceanic-scale interactions on the seasonal modulation of ocean dynamics by the atmosphere. Nat. Commun. **5**: 5636. doi:10.1038/ncomms6636

Silvester, N., B. Alako, C. Amid, and others. 2018. The European nucleotide archive in 2017. Nucleic Acids Res. **46**: D36–D40. doi:10.1093/nar/gkx1125

Taylor, A. G., R. Goericke, M. R. Landry, K. E. Selph, D. A. Wick, and M. J. Roadman. 2012. Sharp gradients in phytoplankton community structure across a frontal zone in the California current ecosystem. J. Plankton Res. **34**: 778–789. doi:10.1093/plankt/fbs036

Taylor, J. R., and R., Ferrari. 2011. Ocean fronts trigger high latitude phytoplankton blooms. Geophys. Res. Lett. **38**: n/a–n/a. http://dx.doi.org/10.1029/2011gl049312

Teeling, H., B. M. Fuchs, D. Becher, and others. 2012. Substrate-controlled succession of marine Bacterioplankton populations induced by a phytoplankton bloom. Science (80-.) **336**: 608–611. doi:10.1126/science.1218344

Teeling, H., B. M. Fuchs, C. M. Bennke, and others. 2016. Recurring patterns in bacterioplankton dynamics during coastal spring algae blooms. Elife **5**: 1–31. doi:10.7554/eLife.11888

Thompson, A. F., A. Lazar, C. Buckingham, A. C. N. Garabato, G. M. Damerell, and K. J. Heywood. 2016. Open-ocean submesoscale motions: A full seasonal cycle of mixed layer instabilities from gliders. J. Phys. Oceanogr. **46**: 1285–1307. doi:10.1175/JPO-D-15-0170.1

Thomsen, S., T. Kanzow, F. Colas, V. Echevin, G. Krahmann, and A. Engel. 2016. Do submesoscale frontal processes ventilate the oxygen minimum zone off Peru? Geophys. Res. Lett. **43**: 8133–8142. doi:10.1002/2016GL070548

von Appen, W.-J., U. Schauer, T. Hattermann, and A. Beszczynska-Möller. 2016. Seasonal cycle of mesoscale instability of the West Spitsbergen current. J. Phys. Oceanogr. **46**: 1231–1254. doi:10.1175/JPO-D-15-0184.1

von Appen, W.-J., C. Wekerle, L. Hehemann, V. Schourup-Kristensen, C. Konrad, and M. H. Iversen. 2018. Observations of a submesoscale cyclonic filament in the marginal ice zone. Geophys. Res. Lett. **45**: 6141–6149. doi:10.1029/2018GL077897

von Appen, W. -J., V. H. Strass, A. Bracher, H. Xi, C. Hörstmann, M. H. Iversen, and A. M. Waite. 2020. High-resolution physical–biogeochemical structure of a filament and an eddy of upwelled water off northwest Africa. Ocean Sci **16**: 253–270. doi:10.5194/os-16-253-2020

von Bodungen, B., M. Wunsch, and H. Fürderer. 1991. Sampling and analysis of suspended and sinking particles in the northern North Atlantic. Washington, DC. Am. Geophys. Union Geophys. Monogr. Ser. **63**: 47–56. doi:10.1029/GM063p0047

Wang, Q., C. Wekerle, X. Wang, and others. 2020. Intensification of the atlantic water supply to the arctic ocean through fram strait induced by Arctic Sea ice decline. Geophys. Res. Lett. **47**: e2019GL086682. doi:10.1029/2019GL086682

Wekerle, C., Q. Wang, S. Danilov, V. Schourup-Kristensen, W.-J. von Appen, and T. Jung. 2017. Atlantic water in the Nordic seas: Locally eddy-permitting ocean simulation in a global setup. J. Geophys. Res. Ocean. **122**: 914–940. doi:10.1002/2016JC012121

Wekerle, C., T. Hattermann, Q. Wang, L. Crews, W.-J. von Appen, and S. Danilov. 2020. Properties and dynamics of mesoscale eddies in Fram Strait from a comparison between two high-resolution ocean–sea ice models. Ocean Sci. **16**: 1225–1246. doi:10.5194/os-16-1225-2020

Wilson, B., O. Müller, E.-L. Nordmann, L. Seuthe, G. Bratbak, and L. Øvreås. 2017. Changes in marine prokaryote composition with season and depth over an arctic polar year. Front. Mar. Sci. **4**: 1–17. doi:10.3389/fmars.2017.00095

Wulff, T., E. Bauerfeind, and W. J. von Appen. 2016. Physical and ecological processes at a moving ice edge in the Fram Strait as observed with an AUV. Deep. Res. Part I Oceanogr. Res. Pap. **115**: 253–264. doi:10.1016/j.dsr.2016.07.001

Acknowledgments

We thank the captain and crew of RV Polarstern expedition PS107, as well as the chief scientist Ingo Schewe. Thanks to Christiane Lorenzen, Sandra Murawski and Nadine Knüppel for biochemical measurements, Malte Schmidt for microscopy counts of phyto- and protozooplankton, Tania Klüver for bacterioplankton flow cytometry, and Halina Tegetmeyer for library preparation and amplicon sequencing of bacterioplankton samples. The authors also thank Federico Baltar for a critical review of the manuscript. This project has received funding from the European Research Council (ERC) under the European Union's Seventh Framework Programme (FP7/2007-2013) research project ABYSS (grant agreement no. 294757) to AB. Microscopic counting was enabled through CAO NERC/BMBF grant 03F0802B. Additional funding came from the Helmholtz Association, specifically for the FRAM infrastructure, from the Max Planck Society, and the Austrian Science Fund (FWF) M-2797 to EF. This study was conducted in the framework of the HGF Infrastructure Program FRAM of the Alfred-Wegener-Institute Helmholtz Centre for Polar and Marine Research. This publication is Eprint ID 53009 of the Alfred Wegener Institute Helmholtz Centre for Polar and Marine Research, Bremerhaven, Germany. Ship time was provided under grant AWI_PS107_07.

Conflict of interest

None declared.

Submitted 05 October 2020
Revised 04 February 2021
Accepted 30 April 2021

Associate editor: Hans-Peter Grossart